

Catalytically active holo *Homo sapiens* adenosine deaminase I adopts a closed conformation

Minh Thu Ma,^{a‡} Maria Rain Jennings,^{b‡} John Blazeczek^{b*} and Raquel L. Lieberman^{a*}

^aSchool of Chemistry and Biochemistry, Georgia Institute of Technology, 901 Atlantic Drive NW, Atlanta, GA 30332, USA, and ^bSchool of Chemical and Biomolecular Engineering, Georgia Institute of Technology, 311 Ferst Drive NW, Atlanta, GA 30332, USA. *Correspondence e-mail: john.blazeczek@chbe.gatech.edu, raquel.lieberman@chemistry.gatech.edu

Received 12 September 2021

Accepted 8 November 2021

Edited by B. Kobe, University of Queensland, Australia

‡ These authors should be considered joint first authors.

Keywords: adenosine deaminase 1; closed conformation; homologs; structural inference.

PDB reference: human adenosine deaminase 1, 7rtg

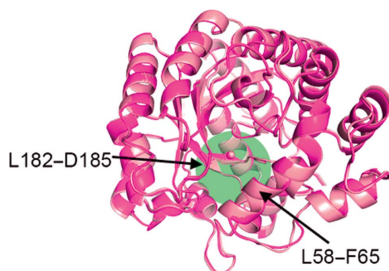
Supporting information: this article has supporting information at journals.iucr.org/d

Homo sapiens adenosine deaminase 1 (HsADA1; UniProt P00813) is an immunologically relevant enzyme with roles in T-cell activation and modulation of adenosine metabolism and signaling. Patients with genetic deficiency in HsADA1 suffer from severe combined immunodeficiency, and HsADA1 is a therapeutic target in hairy cell leukemias. Historically, insights into the catalytic mechanism and the structural attributes of HsADA1 have been derived from studies of its homologs from *Bos taurus* (BtADA) and *Mus musculus* (MmADA). Here, the structure of holo HsADA1 is presented, as well as biochemical characterization that confirms its high activity and shows that it is active across a broad pH range. Structurally, holo HsADA1 adopts a closed conformation distinct from the open conformation of holo BtADA. Comparison of holo HsADA1 and MmADA reveals that MmADA also adopts a closed conformation. These findings challenge previous assumptions gleaned from BtADA regarding the conformation of HsADA1 that may be relevant to its immunological interactions, particularly its ability to bind adenosine receptors. From a broader perspective, the structural analysis of HsADA1 presents a cautionary tale for reliance on homologs to make structural inferences relevant to applications such as protein engineering or drug development.

1. Introduction

Adenosine deaminase enzymes irreversibly convert adenosine and 2-deoxyadenosine (2DA) to inosine and 2-deoxyinosine, respectively, contributing to purine metabolism across prokaryotic and eukaryotic organisms (Fox & Kelley, 1978). The human genome encodes two adenosine deaminases: *Homo sapiens* adenosine deaminase I (HsADA1) and *H. sapiens* adenosine deaminase II (HsADA2) (Wiginton *et al.*, 1986; Zavialov & Engström, 2005). The expression profiles, amino-acid sequences and binding partners of HsADA1 and HsADA2 are distinct, although they share a catalytic mechanism (Zavialov, Yu *et al.*, 2010). HsADA1 is primarily an intracellular enzyme, but can be found as an ectoenzyme in complex with the membrane proteins CD26, an activation and co-stimulatory molecule expressed on the surface of T, B and NK immune-cell subsets, and adenosine receptor (AR) subtypes A₁AR, A_{2A}AR and A_{2B}AR. By contrast, HsADA2 is secreted into serum and can bind proteoglycans (Lee *et al.*, 2020; Zavialov, Gracia *et al.*, 2010).

Early analyses of adenosine deaminase activity in human tissues indicated a maximum in the spleen and high activity in intestinal tissue (Van der Weyden & Kelley, 1976), as well as high activity in thymocytes and circulating lymphocytes (Chechik *et al.*, 1981). These studies did not distinguish between deaminase activity from HsADA1 and HsADA2, but data from the Human Protein Atlas confirm enriched



HsADA1 expression in the blood, intestine and lymphoid tissue (Uhlén *et al.*, 2015). Patients lacking a functional HsADA1 suffer from a severe combined immunodeficiency (ADA-SCID) characterized by reduced B-, NK- and T-cell counts caused by increased deoxyribonucleotide levels that prevent the maturation of lymphocytes and cause their death (Bradford *et al.*, 2017). In ADA-SCID patients, the subsequent defects in lymphocyte-mediated immunity result in eventual fatality if not treated by a bone-marrow transplant or enzyme-replacement therapy (Chan *et al.*, 2005). Long-term administration of a polyethylene glycol (PEG)-conjugated *Bos taurus* adenosine deaminase (BtADA; Pegademase and Elapegademase) benefits ADA-SCID patients by supporting immature lymphocyte development and reconstitution of functional immunity (Chan *et al.*, 2005). Conversely, elevated HsADA1 levels have been associated with inflammatory disease and hematological malignancies, sparking interest in inhibitor development. In particular, the adenosine deaminase inhibitor pentostatin (2'-deoxycoformycin) is used to treat hairy cell leukemia and has been studied as a treatment for graft versus host disease (Kutryb-Zajac *et al.*, 2020).

BtADA has been shown to allosterically modulate the agonist affinity of adenosine receptors A_{2A}AR and A_{2B}AR *in vitro* to increase their sensitivity and heighten intracellular cAMP signaling relevant to immunosuppressed phenotypes (Gracia *et al.*, 2011; Herrera *et al.*, 2001). Further studies with BtADA have established the possibility of a CD26-ADA-A_{2A/B}AR molecular bridge connecting T cells to dendritic cells; however, the immunological significance of the interaction is unknown (Moreno *et al.*, 2018; Herrera *et al.*, 2001). Binding of HsADA1 to A_{2A}AR has also been confirmed *in vitro*, as well as HsADA1-mediated modulation of A₁AR signaling (Gracia *et al.*, 2008, 2013).

HsADA1 is a 41 kDa enzyme with a Zn²⁺ cofactor (Niu *et al.*, 2010; Santisteban *et al.*, 1995). The protein sequence of HsADA1 shares 89% identity with BtADA and 83% identity with murine ADA (MmADA), and catalytic residues are conserved amongst the enzymes (Supplementary Fig. S1). While HsADA1 and BtADA are able to form a complex with CD26, MmADA does not (Richard *et al.*, 2000). Structural studies of BtADA and MmADA reveal a triosephosphate isomerase (TIM)-barrel topology that can adopt 'open' or 'closed' conformations characterized by a subtle shift in a structural gate leading towards the substrate-binding pocket (Niu *et al.*, 2010). Based on these studies, holo (*i.e.* metalated but non-ligand-bound) adenosine deaminase enzymes are thought to adopt the open conformation, as seen in holo BtADA, while the substrate (adenosine or 2DA) and most inhibitors that mimic the substrate are thought to stabilize the closed conformation. Interestingly, holo MmADA appeared to adopt the closed conformation during an initial structural study, although this was attributed to the binding of glycerol from the cryoprotectant (Niu *et al.*, 2010).

While several crystallization studies of BtADA and MmADA have been reported, a crystal structure of holo HsADA1 has yet to be described. Here, we present the structure of holo HsADA, as well as biochemical character-

ization that confirms high activity. Strikingly, although it has a similar overall structure to its homologs, holo HsADA1 adopts an unexpectedly closed conformation with a noticeable shift in its structural gate compared with holo BtADA. Previously, adenosine deaminase enzymes were expected to maintain an open conformation until ligand binding. Our structural result has implications for future inhibitor development and for the immunological functions of HsADA1.

2. Materials and methods

2.1. Macromolecule production and characterization

2.1.1. Cloning of the human adenosine deaminase 1-containing plasmid. The gene sequence for HsADA1 (UniProt P00813) was codon-optimized for *Escherichia coli* expression and synthesized as a linear DNA fragment by Twist Biosciences. All oligonucleotide primer sequences were purchased from Eurofins Genomics and all restriction enzymes were purchased from New England Biolabs. To add the first C-terminal Gly-Gly-His-His-His-His-His-His-Gly-Gly sequence (GG-6His-GG), two polymerase chain reaction (PCR) steps were employed. Firstly, using the HsADA1 gene as the template and oligonucleotide primer sequences (forward, 5'-AACTTTAAGAAGGAGATATACCATGGCTCAAACCTCCGGCCTTCGAC-3'; reverse, 5'-TGGTGGTGATGATGACCGCCCAAGTTCTGGCCCGCGCTTG-3'), the first portion of the GG-6His-GG sequence was appended to the C'-terminus of the HsADA1 gene. The second PCR step used the first PCR as a template and additional primers (forward, 5'-AACTTTAAGAAGGAGATATACCATGGCTCAAACCTCCGGCCTTCGAC-3'; reverse, 5'-TCGAGTGCGGCCGCAAGCTTGTCTGACTTAGCCGCCGTGATGTGGTGATGATGACCGCC-3') to complete the addition of GG-6His-GG. This PCR product was subsequently inserted into the pET-28a(+) backbone between the NcoI and SalI restriction sites through Gibson assembly. Next, a second hexahistidine tag was appended to the HsADA1-GG-6His-GG sequence by amplifying the region (forward, 5'-GGAATTGTGAGCGGATAACAATTCCCC-3'; reverse, 5'-CAGTGGTGGTGGTGGTGGTGGCCGCGCGTGATGGTGGT-3') with overhang for the C'-terminal hexahistidine tag flanking the XhoI site in the pET-28a(+) multiple cloning site. This fragment was inserted between the NcoI and XhoI sites of pET-28a(+) using Gibson assembly for a final plasmid construction of pET-28a(+) HsADA1-GG-6His-GG-6His. To insert a Tobacco etch virus (TEV) protease cleavage site between the HsADA1 and GG-6His-GG-6His sequences, the entirety of the plasmid was constructed and assembled from three fragments. Firstly, the TEV site was appended to the C'-terminus of the HsADA1 gene using pET-28a(+) HsADA1-GG-6His-GG-6His as a template and oligonucleotide primers (forward, 5'-GGGGAATTGTGAGCGGATAACAATTCCCC-3'; reverse, 5'-GCCGCGTGATGGTGGTGATGATGACCGCCGATTGGAAGTACAGGTTCTCAAGTTCTGGCCCGCGCTTG-3') to generate the first PCR product. The second PCR fragment also made use of

purchased from Sigma–Aldrich), 1 mM phenylmethylsulfonyl fluoride (Thermo Scientific), 25 U ml⁻¹ Universal Nuclease (Pierce) and 1 mg ml⁻¹ lysozyme (Thermo Scientific). Frozen pellets were resuspended at a ratio of 5 ml chilled lysis buffer to 1 g pellet. The pellets were gently spun with a magnetic stir bar at 4°C until resuspended. The resuspended cells were sonicated using a QSonica 500 Sonicator with a 1/2" tip attachment at 40% amplitude for a total of 30 min of sonication with cycles of 5 s on and 1 s off. The lysate was aliquoted into 50 ml conical tubes (Eppendorf) and centrifugated for an hour at 20 000g and 4°C. The clarified lysate was passed through sterile 0.22 µm GD/X Whatman filters (GE Healthcare) and loaded into a 150 ml Superloop (Cytiva). A 5 ml HisTrap High Performance nickel-affinity column (Cytiva) on an ÄKTA pure system (Cytiva) at 4°C was used to purify HsADA1-TEV-GG-6His-GG-6His. After equilibrating the column with five column volumes (CV) of buffer A (20 mM sodium phosphate pH 7.4, 300 mM NaCl, 20 mM imidazole), the sample was applied and washed with 10 CV buffer A, followed by elution with a linear gradient from 0% to 100% buffer B (20 mM sodium phosphate pH 7.4, 300 mM NaCl, 500 mM imidazole) over 15 CV. The fractions were analyzed by SDS–PAGE and pure fractions were pooled, sterile filtered using a 0.22 µm filter (Fisher) and concentrated using Amicon Ultra-15 Centrifugal Filter Units with Ultracel-10 membrane (Millipore). Concentrated HsADA1-TEV-GG-6His-GG-6His was buffer-exchanged into chilled phosphate-buffered saline (PBS) pH 7.4 using HiTrap Desalting Columns (Cytiva). The $A_{280\text{ nm}}$ of the protein was determined using a NanoDrop One/One^C UV–Vis spectrophotometer (Thermo Scientific). The Expasy tools (Wilkins *et al.*, 1999) were used to calculate molecular masses and extinction coefficients for full-length and cleaved HsADA1.

2.1.4. Cleavage of HsADA1-TEV-GG-6His-GG-6His. HsADA1-TEV-GG-6His-GG-6His was mixed with 6His-TEV(S219V)-Arg₅ in a 10 mg:1 mg ratio. 6His-TEV(S219V)-Arg₅ was produced using *E. coli* BL21(DE3) CodonPlus-RIL cells containing the pRK793 plasmid as described previously (Tropea *et al.*, 2009). The mixture was gently turned end-over-end at 4°C for 16 h and sterile filtered with GD/X Whatman 0.22 µm filters. The mixture was then diluted tenfold with buffer A and applied onto a 150 ml Superloop. The protocol described above was used to obtain near-homogeneous, untagged HsADA1, and the column flowthrough was passed through a 0.22 µm filter, concentrated using a 10 kDa device and buffer-exchanged into PBS pH 7.4 using a HiTrap Desalting Column as described above. The purity of the untagged HsADA1 was assessed by SDS–PAGE and the concentration was determined by measurement of the $A_{280\text{ nm}}$.

2.1.5. Kinetic analysis of HsADA1. Kinetic parameters for HsADA1 were determined via a 96-well assay method using substrate concentrations ranging from 0 to 250 µM adenosine and from 0.001 to 0.005 µM HsADA1. In a 96-well UV-Transparent Microplate (Corning), 160 µl of 1.25× substrate solution was added to a 40 µl well containing 5× enzyme solution. The absorbance at 265 nm, as a readout of the adenosine level, was monitored using a BioTek Synergy HT

96-well plate spectrometer. The adenosine degradation rate was calculated from the linear portion of the raw reaction curves corresponding to less than 10% substrate degradation. Nonlinear regression analysis was performed with *OriginPro* 2021. The pH of each buffer solution was established with a 50 mM buffer salt ratio corresponding to the following pH ranges: (i) pH 3.0–5.4, citric acid:sodium citrate, (ii) pH 5.8–8.0, sodium phosphate monobasic:sodium phosphate dibasic, and (iii) pH 9.2–10.8, sodium carbonate:sodium bicarbonate.

2.1.6. Differential scanning fluorimetry. Differential scanning fluorimetry was performed using a NanoTemper PROMETHEUS NT.48 NanoDSF. The protein was loaded into PROMETHEUS NT.48 glass capillaries at a concentration of 1 mg ml⁻¹ in 50 mM sodium phosphate pH 7.4. The *NanoTemper PR.ThermoControl* version 2.1.5 software was used to visualize the absorbance curves at 330 and 350 nm, the curve of the 330 nm:350 nm absorbance ratio and the first derivative of the absorbance-ratio curve as the temperature was ramped from 20 to 90°C at a rate of 0.5°C min⁻¹.

2.2. Crystallization

Purified, cleaved HsADA1 was exchanged into 10 mM HEPES pH 7.5, 150 mM NaCl and concentrated to 23 mg ml⁻¹ using an Amicon filtration unit with a 3 kDa molecular-weight cutoff using six concentration and dilution steps. Crystals grew within ~6 months at 20°C in a sitting drop consisting of a 1:1(v:v) ratio of 23 mg ml⁻¹ HsADA1 and a reservoir solution consisting of 0.49 M sodium phosphate monobasic monohydrate, 0.91 M potassium phosphate dibasic pH 6.9. Crystals were cryoprotected by brief incubation in ~2 M lithium sulfate followed by flash-cooling in liquid nitrogen. Crystallization information is summarized in Table 2.

2.3. Data collection and processing

Diffraction data were collected on the Southeast Regional Collaborative Access Team (SER-CAT) 22-ID beamline at the Advanced Photon Source (APS) and were processed using *HKL-2000* (Otwinowski & Minor, 1997). The crystals were not singular, which affected the overall completeness of the data set. Data-collection and processing statistics are summarized in Table 3.

2.4. Structure solution and refinement

The structure was solved by molecular replacement in *Phaser* (McCoy *et al.*, 2007) using the polypeptide chain from PDB entry 3iar (Structural Genomics Consortium, unpublished work) as a search model. The HsADA1 model was iteratively built and refined using *Coot* (Casañal *et al.*, 2020) and *phenix.refine* (Liebschner *et al.*, 2019). Figures were prepared in *PyMOL*. The structure was deposited in the PDB with accession code 7rtg. Refinement statistics are summarized in Table 4. A representative image of the electron density of the final model is shown in Supplementary Fig. S2A.

Table 2
Crystallization.

Method	Vapor diffusion, sitting drop
Plate type	Intelli-Plate 96-3 LVR
Temperature (K)	293
Protein concentration (mg ml ⁻¹)	23
Buffer composition of protein solution	19 mM HEPES pH 7.5, 150 mM NaCl
Composition of reservoir solution	0.49 M sodium phosphate monobasic monohydrate, 0.91 M potassium phosphate dibasic pH 6.9
Volume and ratio of drop	0.33 µl, 1:1
Volume of reservoir (µl)	50

Table 3
Data collection and processing.

Values in parentheses are for the outer shell.

Diffraction source	SER-CAT 22-ID, APS
Wavelength (Å)	1.0
Temperature (K)	100
Detector	Dectris EIGER X16M
Space group	<i>P</i> ₂ ₁
<i>a</i> , <i>b</i> , <i>c</i> (Å)	80.91, 49.52, 89.09
α , β , γ (°)	90, 96.18, 90
Resolution range (Å)	42.17–2.59 (2.68–2.59)
Total No. of reflections	42494 (874)
No. of unique reflections	17712 (463)
Completeness (%)	75.67 (21.09)†
Multiplicity	2.4 (1.4)
CC _{1/2}	0.98 (0.76)
CC*	0.99 (0.93)
$\langle I/\sigma(I) \rangle$	7.39 (1.75)‡
<i>R</i> _{merge}	0.1201 (0.3697)
<i>R</i> _{meas}	0.1495 (0.5042)

† Completeness issues derive from multiple lattice issues in the crystalline sample. ‡ $\langle I/\sigma(I) \rangle$ falls below 2.0 at 2.7 Å resolution. Data were included to 2.6 Å resolution because the CC_{1/2} value in the highest resolution bin is 0.75, despite it only being 21% complete.

3. Results

3.1. Kinetic characterization of high-purity HsADA1

We expressed a codon-optimized HsADA1 gene, modified to append a C-terminal TEV protease site and hexahistidine tags, in *E. coli* T7 Express. SDS-PAGE analysis shows that HsADA1 is >99% pure after nickel-affinity chromatography, with an expected decrease in molecular weight after TEV cleavage from 43.5 to 41.6 kDa (Fig. 1a). Fractionation of pure cleaved HsADA1 by size-exclusion chromatography confirms that HsADA1 is predominantly monomeric in solution, with only a small dimeric HsADA1 population (Fig. 1b). Expression yields range from 10 to 15 mg protein per litre at 95% purity or greater following affinity chromatography, similar to those obtained for MmADA (Mohamedali *et al.*, 1996).

We evaluated the kinetics of HsADA1 with its preferred substrate, adenosine. Nonlinear regression analysis revealed catalytic parameters (Fig. 1c; $k_{\text{cat}} = 93.7 \pm 2.0 \text{ s}^{-1}$ and $K_{\text{m}} = 13.7 \pm 1.0 \text{ }\mu\text{M}$, $k_{\text{cat}}/K_{\text{m}} = 7.15 \times 10^6 \text{ M}^{-1} \text{ s}^{-1}$) that were similar to the reported activities of BtADA ($k_{\text{cat}} = 385 \text{ s}^{-1}$ and $K_{\text{m}} = 43 \text{ }\mu\text{M}$, $k_{\text{cat}}/K_{\text{m}} = 8.95 \times 10^6 \text{ M}^{-1} \text{ s}^{-1}$) and MmADA ($k_{\text{cat}} = 240 \text{ s}^{-1}$ and $K_{\text{m}} = 21 \text{ }\mu\text{M}$, $k_{\text{cat}}/K_{\text{m}} = 1.14 \times 10^7 \text{ M}^{-1} \text{ s}^{-1}$) and nearly two orders of magnitude higher than for HsADA2 ($k_{\text{cat}} = 88 \text{ s}^{-1}$ and $K_{\text{m}} = 2 \text{ mM}$) (Wang *et al.*, 2012; Sideraki *et al.*, 1996; Zavialov & Engström, 2005). Previous characterization of the catalytic activity of recombinant HsADA1 ($k_{\text{cat}} =$

Table 4
Structure solution and refinement.

Values in parentheses are for the outer shell.

Resolution range (Å)	42.17–2.59 (2.68–2.59)
Completeness (%)	75.67 (21.09)
σ Cutoff	7.39 (1.75)
No. of reflections, working set	16809 (463)
No. of reflections, test set	1679 (46)
Final <i>R</i> _{cryst}	0.2013 (0.3845)
Final <i>R</i> _{free}	0.2607 (0.4647)
No. of non-H atoms	
Total	5588
Protein	5562
Ligand	2
Solvent	24
Protein residues	701
R.m.s. deviations	
Bonds (Å)	0.008
Angles (°)	1.60
Average <i>B</i> factors (Å ²)	
Overall	42.34
Protein	42.39
Ligand	39.43
Solvent	31.27
Ramachandran plot	
Most favored (%)	95.98
Allowed (%)	3.59
Outliers (%)	0.43

190 s⁻¹ and $K_{\text{m}} = 26 \text{ }\mu\text{M}$, $k_{\text{cat}}/K_{\text{m}} = 7.31 \times 10^6 \text{ M}^{-1} \text{ s}^{-1}$) is in agreement with our results (Liu *et al.*, 2016). The activities of tagged ($k_{\text{cat}} = 94.6 \pm 3.5 \text{ s}^{-1}$ and $K_{\text{m}} = 12.4 \pm 1.6 \text{ }\mu\text{M}$, $k_{\text{cat}}/K_{\text{m}} = 7.62 \times 10^6 \text{ M}^{-1} \text{ s}^{-1}$) and cleaved HsADA1 (Fig. 1c) are nearly identical, and the thermal stability is similarly unaffected [Fig. 1d; T_{m} before removal = $61.7 \pm 0^\circ\text{C}$ ($n = 3$), T_{m} after cleavage = $60.1 \pm 0^\circ\text{C}$ ($n = 3$)]. Thus, the hexahistidine tag and its removal does not interfere with catalysis or stability. Reactions conducted in a pH range between 3.0 and 10.8 demonstrate broad activity, with optimal pH values for the degradation of adenosine by HsADA1 in the physiological pH range between 6.0 and 8.0 (Fig. 1e).

3.2. Overall structure of holo HsADA1

The HsADA1 structure was solved at 2.6 Å resolution by molecular replacement (Tables 3 and 4, Supplementary Fig. S2a). HsADA1 adopts the expected α/β -barrel architecture and TIM-barrel topology (Fig. 2a). The two copies of HsADA1 in the asymmetric unit are indistinguishable (r.m.s.d. of 0.34 Å) except for minor loop configurations. In addition, the calculated contact surface area (Krissinel & Henrick, 2007) between the two polypeptides is low ($\sim 600 \text{ }\text{Å}^2$), in line with chromatographic results indicating that HsADA1 is predominantly monomeric (Fig. 1b). Both monomers in the asymmetric unit have a similarly organized active site with a copurified Zn²⁺ ion (Fig. 2b), which is expected to lower the p*K*_a of water to facilitate catalysis (Mohamedali *et al.*, 1996).

3.3. Structural comparisons of holo HsADA1 reveal that it adopts a closed conformation

When they are unbound by substrate, mammalian adenosine deaminase enzymes are thought to adopt an 'open'

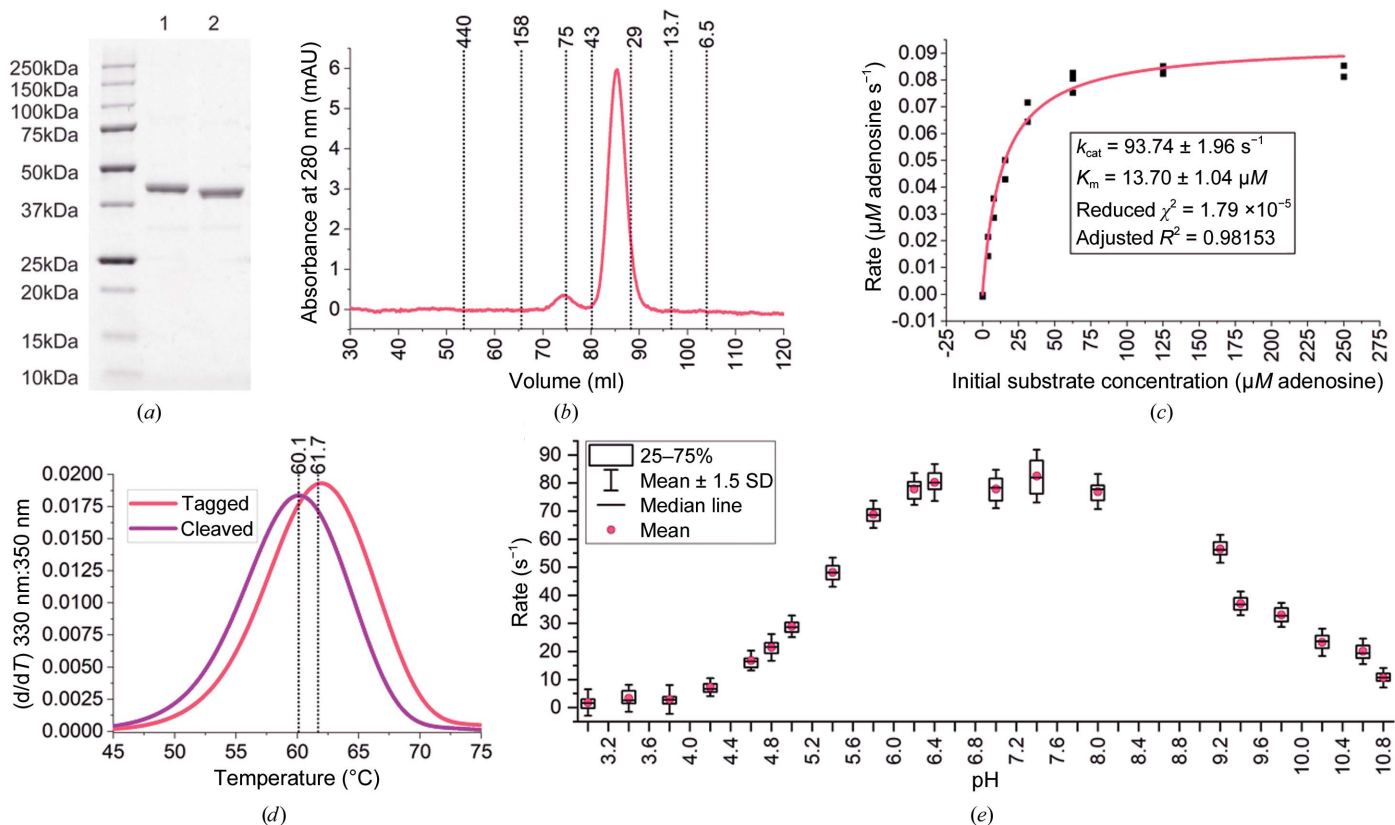


Figure 1 Functional properties of purified HsADA1. (a) SDS–PAGE analysis of HsADA1 before (lane 1) and after (lane 2) cleavage of the His tag with TEV protease, showing the expected decrease in molecular mass. (b) Size-exclusion chromatography elution profile for cleaved HsADA1. (c) Michaelis–Menten kinetic parameters of cleaved HsADA1 at pH 7.4, which agree with previously reported values. (d) Stability of tagged and cleaved HsADA1 obtained from differential scanning fluorimetry. The melting temperature was determined as the inflection point of the first derivative with respect to temperature of the 330 nm:350 nm absorbance ratio. (e) His-tagged HsADA1 activity as a function of pH condition ($n = 32$ per pH condition). Due to the different concentrations of enzyme necessary to obtain a robust signal for each pH condition, the original rate calculation (determined by linear regression from the initial 10% of substrate degradation) in units of μM adenosine per second was divided by the concentration of HsADA1 in μM to obtain a normalized unit of s^{-1} .

conformation characterized by the location of the Leu58–Phe65 α -helix and Leu182–Asp185 loop, which make up a structural gate leading from the surface to the active site (Fig. 2a; Gracia *et al.*, 2013). Substrate binding is expected to be accompanied by a shift of the α -helix towards the loop,

reducing access to the active site as the enzyme adopts the ‘closed’ conformation. Several lines of data support the conclusion that holo HsADA1 adopts an unexpected, closed conformation. Firstly, comparison of holo HsADA1 with the closed conformation adopted by the 2DA/ Ni^{2+} -bound structure (Figs. 3a and 3b; PDB entry 3iar, r.m.s.d. of 0.37 Å) reveals near-perfect overlap in the conformation of their structural gates. The Ni^{2+} ion, which replaces Zn^{2+} , is expected to abolish the catalytic activity (McCall *et al.*, 2000; Fig. 3b). The main difference between holo HsADA1 and 2DA/ Ni^{2+} -bound HsADA1 is that no electron density was observed for amino acids 354–364 distal to the active site in holo HsADA1. In the 2DA/ Ni^{2+} -bound structure these residues form an α -helix (Fig. 3c). These residues appear to have been proteolyzed prior to crystallization, as they are incompatible with the crystal lattice, clashing with the helix comprising Ala43–Ile50 on a crystallographically

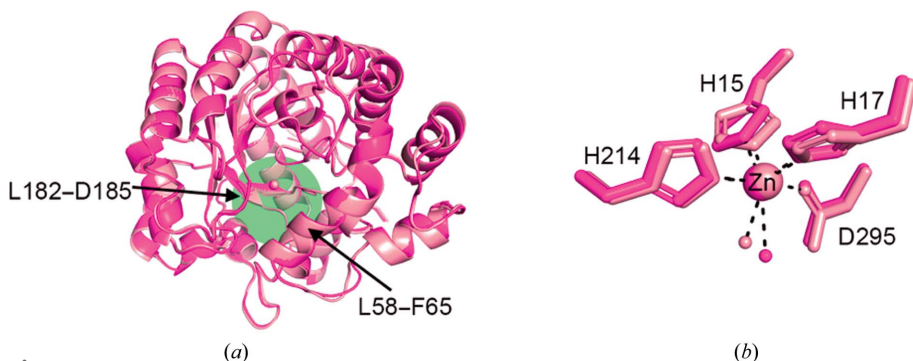


Figure 2 Structure of holo HsADA1. (a) Overlay of holo HsADA1 monomers in the crystal asymmetric unit. Monomer A (magenta) and monomer B (light pink) exhibit only minor structural differences, with an overall r.m.s.d. of 0.34 Å. The green circle indicates the structural gate formed by residues Leu58–Phe65 and Leu182–Asp185. (b) Enlarged view of the zinc-binding regions of monomers A and B. The side chains of the active-site residues are shown as sticks along with the coordinating water molecules. Dashed lines represent coordinating interactions with zinc.

related molecule (Supplementary Fig. S2*b*). These residues do not affect activity ($k_{\text{cat}} = 104 \pm 1.8 \text{ s}^{-1}$ and $K_{\text{m}} = 23.0 \pm 1.3 \mu\text{M}$, $k_{\text{cat}}/K_{\text{m}} = 4.53 \times 10^6 \text{ M}^{-1} \text{ s}^{-1}$; Supplementary Fig. S2*c*). These terminal residues are absent in MmADA1

(Supplementary Fig. S1), are not visible in the BtADA structures available to date (not shown) and are poorly predicted by *AlphaFold* (Jumper *et al.*, 2021; Mirdita *et al.*, 2021; Tunyasuvunakool *et al.*, 2021; Supplementary Fig. S2*d*).

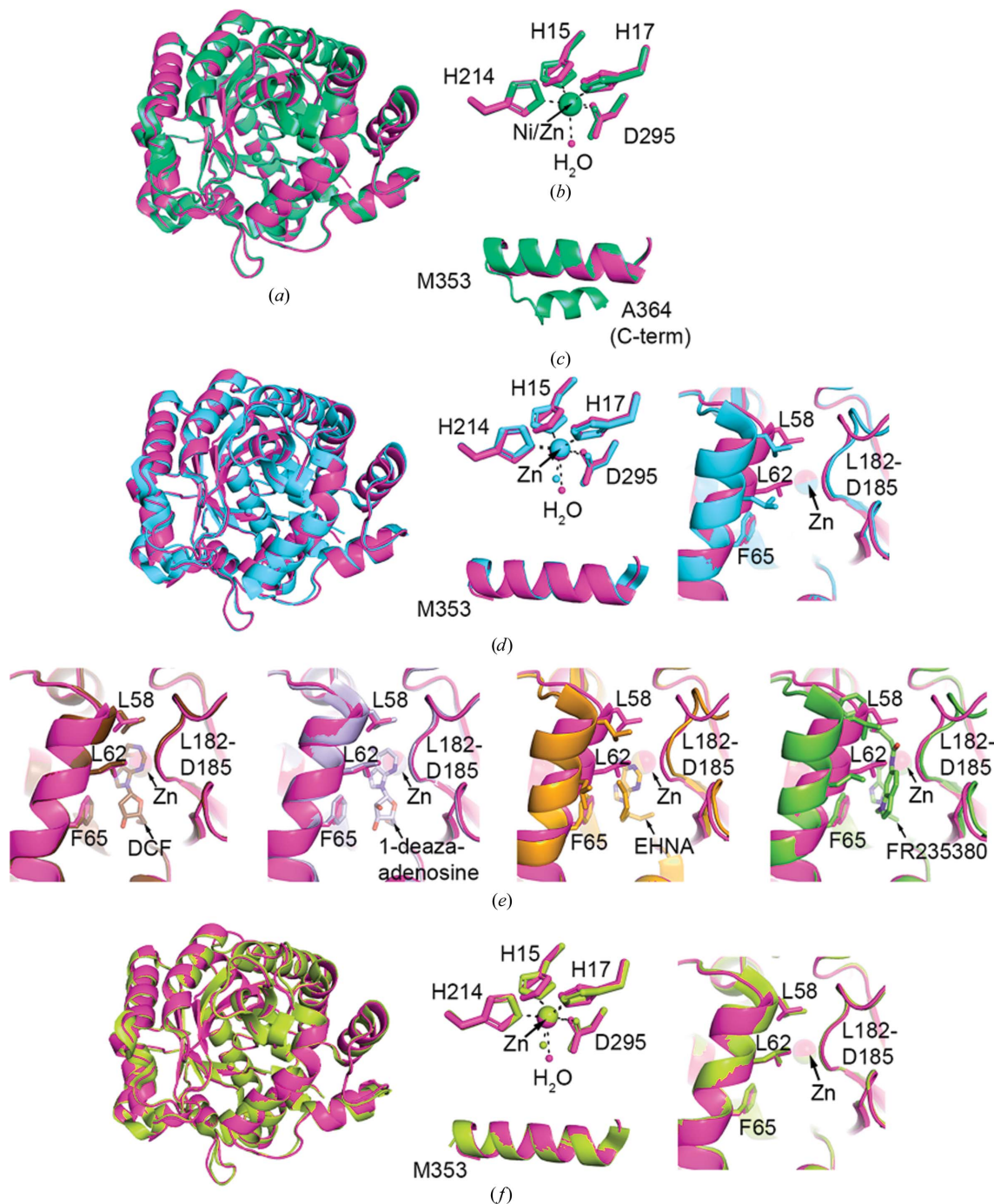


Figure 3

Comparison of HsADA1 with other structures of mammalian ADA1 enzymes. (a) Overlay of holo HsADA1 monomer A (magenta) with the unpublished structure of substrate/ Ni^{2+} -bound HsADA1 (PDB entry 3iar, lime green). (b) Comparison of Zn^{2+} and Ni^{2+} coordination in HsADA1 and PDB entry 3iar, respectively. (c) Enlarged view of the C-terminal helix (residues 354–364) that is present in PDB entry 3iar but absent in HsADA1. (d) Overlay of holo HsADA1 monomer A (magenta) and holo BtADA (cyan) with enlarged views of the Zn^{2+} environment, C-terminal helix and structural gate. HsADA1 adopts an open conformation with shifts in Leu58, Leu62 and the Leu182–Asp185 loop compared with the closed conformation of holo BtADA. (e) Comparison of the structural gate of HsADA1 monomer A (magenta) with MmADA complexed with DCF (brown) and 1-deaza-adenosine (light blue) and with BtADA complexed with EHNA (orange) and FR235380 (lime green). HsADA1 has similar structural features at the catalytic gate to the closed conformation adopted by MmADA–inhibitor complexes, while displaying shifts in this region from the open conformation adopted by BtADA–inhibitor complexes. (f) Overlay of monomer A (magenta) with holo MmADA (yellow) with enlarged views of the Zn^{2+} environment, C-terminal site and structural gate. The structural features of the catalytic gate of HsADA1 overlap closely with those of holo MmADA.

Secondly, in comparison with holo BtADA1 (PDB entry 1vfl; Kinoshita *et al.*, 2005), which adopts the canonical open conformation, the Leu58–Phe65 helix in holo HsADA1 tilts 2–3.5 Å to shrink the opening of the structural gate (Fig. 3*d*). Thirdly, we compared holo HsADA1 with structures of BtADA1 and MmADA1 bound to inhibitors that stabilize either the closed [MmADA1 in complex with 2'-deoxycoformycin (DCF; PDB entry 1a4l; Wang & Quiocho, 1998) or 1-deaza-adenosine (1-DAA; PDB entry 1add; Wilson & Quiocho, 1993)] or open [BtADA1 in complex with EHNA (PDB entry 2z7g; Kinoshita *et al.*, 2008) or FR235380 (PDB entry 1qxl; Terasaka *et al.*, 2004)] enzyme conformations (Fig. 3*e*). The structural gate of holo HsADA1 shows clear alignment with the closed conformation of the DCF- or

1-DAA-bound enzyme, and a noticeable shift away from the open conformation seen in the EHNA- or FR232580-complexed enzyme. Finally, the structural gate configuration of holo HsADA1 is similar to that of holo MmADA (PDB entry 3mvi; Niu *et al.*, 2010; Fig. 3*f*), which has a bound glycerol near the gate (however, see below).

3.4. Analysis of crystal contacts in holo HsADA1, MmADA and BtADA rules out a possible crystallographic artifact of the closed conformation

Next, we considered the role of crystal packing in the conformation of the structural gate configuration across the bovine, mouse and human holo ADA structures. In all three structures there is a crystal contact near the structural gate helix (Leu58–Phe65) involving Tyr67 (Supplementary Fig. S1, Fig. 4*a*). The side chain of Tyr67 forms contacts with different residues in crystallographically related protein copies (Figs. 4*b–e*): in holo HsADA1 the interaction is with the main-chain carbonyl O atoms of Pro354 and Pro355 (Fig. 4*b*), in holo MmADA it is a water-mediated contact with Glu345 (Fig. 4*c*) and in holo BtADA the interaction is with Lys207 (Fig. 4*d*). In HsADA1 and MmADA, there are no other contacts within in the structural gate helix. By contrast, in holo BtADA there is a crystal contact within the structural gate helix. The side chain of Asp61 forms a contact with Ser207 from a crystallographically related molecule (Fig. 4*d*). We do not know whether the open conformation of BtADA was previously considered to be a possible crystallographic artifact, as this contact may artificially induce or stabilize the open conformation in the lattice. In the available closed conformation of BtADA observed in the structure in complex with 6-hydroxyl-1,6-dihydropurine (HDPR; PDB entry 1krm; Kinoshita *et al.*, 2003), Asp61 does not make a crystal contact (Fig. 4*e*). Taken together, the closed conformation adopted by holo HsADA1 is not constrained by the crystal lattice.

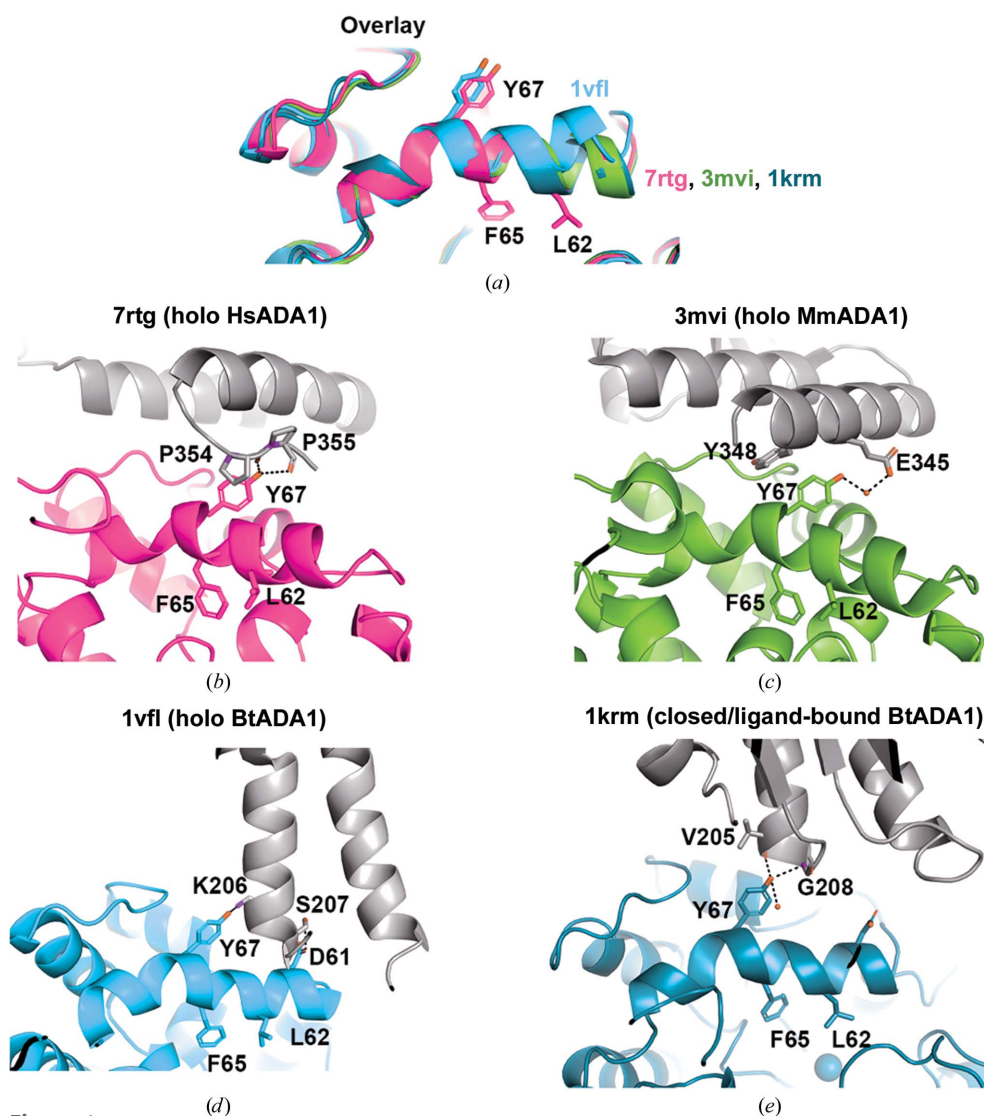


Figure 4 Crystal contact analysis. (a) Overlay of four key illustrative structures in the region of the structural gate helix comprising residues 58–65. In all four structures Tyr67 participates in crystal contacts and is in a similar position. (b) Crystal contacts for holo HsADA1 showing polar contacts with the Pro354 and Pro355 main-chain carbonyls. (c) Crystal contacts for holo MmADA showing a water-mediated contact with Glu345. (d) Crystal contacts for holo BtADA showing interaction between Tyr67 and Lys206 as well as between Asp61 and Ser207. (e) Crystal contacts in the closed-conformation structure of BtADA showing contact only between Tyr67 and the main-chain atoms of Val205 and Gly208. Dashed lines represent contacts between 2.6 and 3.5 Å.

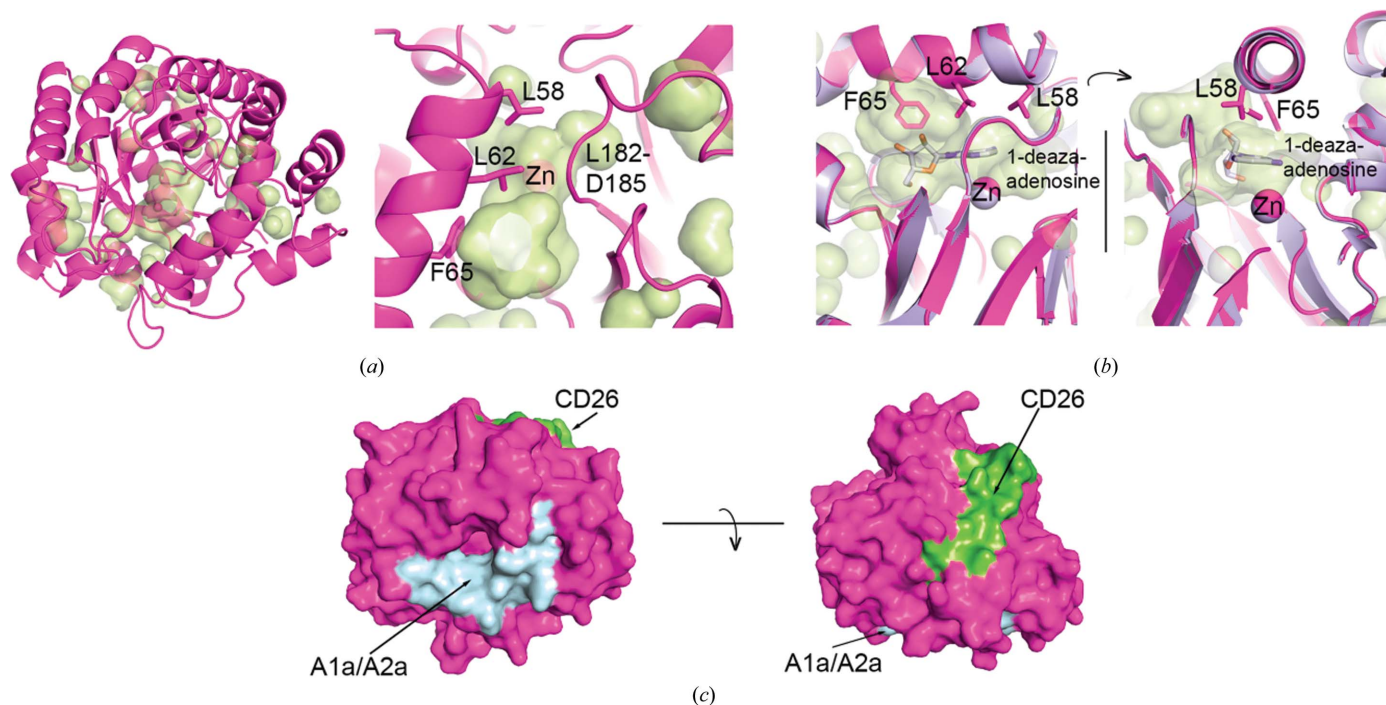


Figure 5

Cavity and receptor-binding site analysis. (a) Left panel, overview of holo HsADA1 with solvent cavities shown in pale yellow. Right panel, enlargement of the structural gate. (b) Two orientations of the structural gate overlaid with PDB entry 1add in which 1-deaza-adenosine is bound to MmADA, showing good agreement with the cavity in HsADA1. (c) Surface representation of the expected CD26 and adenosine receptor binding sites of HsADA1.

3.5. Analysis of holo HsADA1 substrate- and receptor-binding sites

Cavity analysis of holo HsADA1 highlights the substrate-binding pocket and the extent of its accessibility through the ‘closed’ catalytic gate (Figs. 5*a* and 5*b*). There is a pocket at the equivalent site for substrate or inhibitor binding in other mammalian ADA enzymes (Fig. 5*b*). In support of the notion that a conformational change to a more open state is required to access the substrate-binding site, computational docking fails to find a pose in the active site below the closed gate, whereas the equivalent docking to holo BtADA1, in an open conformation, is successful (not shown).

Functionally, the conformation of the structural gate has been speculated to be important for the binding of HsADA1 to the adenosine receptors A₁AR and A_{2A}AR (Gracia *et al.*, 2013). The residues implicated in AR binding, Leu58–Ile72 and Ala184–Ile188, rim two sides of the entrance to the HsADA1 active site (Fig. 5*c*), overlapping with the structural gate. By contrast, the HsADA1 residues implicated in its interaction with the costimulatory CD26 molecule, Pro126–Asp143, are located on a helix remote from the structural gate on the opposite face of the protein (Fig. 5*c*; Richard *et al.*, 2000). Thus, HsADA1 should be able to simultaneously interact with multiple binding partners, as has previously been proposed (Moreno *et al.*, 2018; Gracia *et al.*, 2013; Pacheco *et al.*, 2005).

3.6. Comparison of HsADA1 and HsADA2

HsADA2 has a much higher K_m for adenosine than HsADA1 (millimolar versus low micromolar), is larger and

forms a homodimer. Dimerization of HsADA2 occurs primarily through interactions between regions that are not conserved in HsADA1 (Zavialov, Yu *et al.*, 2010). The overall TIM-barrel fold and coordination to the Zn²⁺ cofactor are conserved in both enzymes (r.m.s.d. of 4.7 Å; Figs. 6*a* and 6*b*) despite low primary-sequence homology (22% sequence identity; Supplementary Fig. S3). One relevant loop with a vastly different conformation for each enzyme consists of amino acids 107–126 in HsADA1 (homologous to amino acids 221–235 in HsADA2), referred to in previous work as the ‘β2–α2’ loop (Fig. 6*a*; Zavialov, Yu *et al.*, 2010). In HsADA1, the β2–α2 loop participates in hydrophobic contacts with the Leu58–Phe65 helix of the active-site gate, but these interactions are precluded in the configuration of the β2–α2 loop present in HsADA2, which adopts the same ‘open’ conformation as a holo enzyme or when bound by coformycin (CF; Fig. 6*c*). Thus, the conformation of the β2–α2 loop may affect the open and closed conformations of the structural gate in human ADAs.

4. Discussion

Here, we presented the biochemical characterization and crystal structure of holo HsADA1, which exhibits pleiotropic effects on immune signaling by hydrolysis of its substrate adenosine and by binding to CD26 and ARs. We overcame previous limitations of preparative expression in *E. coli* (Bhaumik *et al.*, 1993; Gracia *et al.*, 2013) by using an *E. coli* codon-optimized gene for HsADA1 and a robust protein-production strain. This process resulted in impressive

expression yields that eased characterization of the enzyme (Fig. 1).

For 25 years, insights into the structure and function of HsADA1 have been derived from studies of the close homologs MmADA (83% identical to HsADA1) and BtADA (89% identical to HsADA1) (Bhaumik *et al.*, 1993). Early observations based on inhibitor-bound MmADA and BtADA structures noted that there was no entry point to the active site that was wide enough to allow inhibitor access, implying that a conformational change had occurred upon binding that closed off the active site. The first holo structure, that of BtADA, appeared to capture this implicated ‘open’ conformation. In holo BtADA there is a ~ 3 Å lateral shift at the top of the helix gating access to the active site compared with the same helix in the structure of BtADA complexed with HDPR (Kinoshita *et al.*, 2003). The idea that mammalian ADA enzymes convert from an ‘open’ conformation in the holo form to a closed state upon binding substrates led to the conclusion that holo MmADA adopted a ‘closed’ conformation because of a fortuitously bound glycerol molecule (Niu *et al.*, 2010); to our knowledge, the open conformation of MmADA has not been experimentally observed.

Our structure of holo HsADA1, which adopts the ‘closed’ conformation in common with holo MmADA, raises new doubts that the ‘open’ structural gate conformation is stable across mammalian ADAs. Crystal-packing analysis indicates that a conserved structural gate helix residue, Asp61, is involved in a crystal contact in holo BtADA but not in holo HsADA1, holo MmADA or HDPR-bound BtADA1. In addition, *AlphaFold* predicts holo BtADA to be in the closed conformation (Supplementary Fig. S2*d*). The closed conformation appears to be readily trapped crystallographically in holo MmADA and HsADA1, even though the opportunity for a crystal contact employing Asp61 is available across the orthologs. The role of crystal contacts in the observed conformation of mammalian ADA enzymes should be explored further. For example, it is possible that the open conformation seen for EHNA and FR235380 bound to BtADA is because of lattice energetics, and only the specific stabilizing interactions endowed by HDPR binding can disfavor the crystal contact with Asp61 to stabilize the ~ 4 Å shifted closed conformation. In this new context, the resemblance of holo HsADA1 to holo MmADA indicates that no conformational change occurs after the binding of DCF or 1-DAA to holo MmADA. These observations should prompt direct experiments with MmADA and HsADA1 to determine whether EHNA or FR235380 can stabilize an open state, including, critically, in solution.

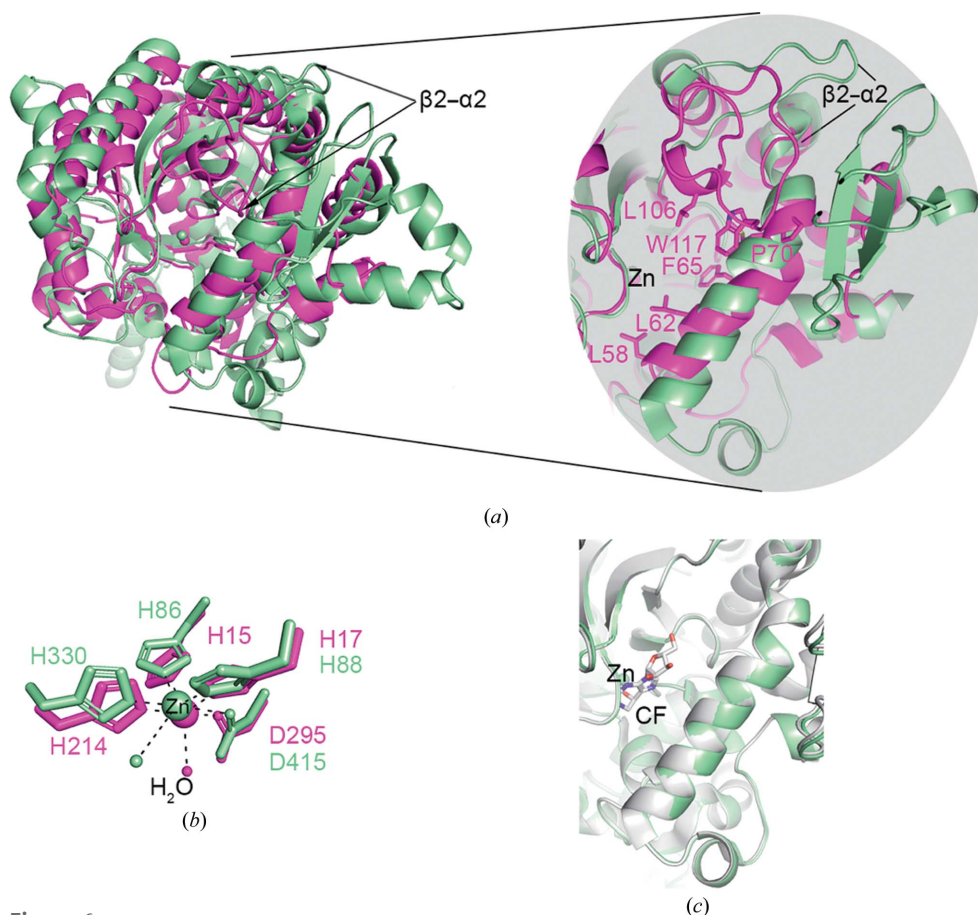


Figure 6

Comparison of HsADA1 with HsADA2. (a) Superposition of monomer A (magenta) of HsADA1 and holo HsADA2 (light green; PDB entry 3lgd), with arrows indicating the location of the $\beta 2$ - $\alpha 2$ loop. Inset, enlarged view of the $\beta 2$ - $\alpha 2$ loop showing interaction of $\beta 2$ - $\alpha 2$ with the helix of the structural gate in HsADA1 but not in HsADA2. (b) Enlarged view of the Zn^{2+} coordination environment. (c) Enlarged view of the structural gate showing that nonligated HsADA2 and CF-bound HsADA2 (gray; PDB entry 3lgg) adopt the same conformation, which is analogous to the open conformation of BtADA (see Fig. 3e).

Alternatively, BtADA may be conformationally distinct from MmADA and HsADA1. Firstly, although the three homologous sequences are >80% identical, including all of the residues that line the active site, the protein sequence of the holo BtADA structure differs by eight residues compared with the protein sequence deposited with UniProt, in which four positions have been substituted by the residues in HsADA1 (Supplementary Fig. S1). The origin of these substitutions is not clear, but may come from challenges in the expression or purification of BtADA1 for structure determination or from natural genetic diversity within the *B. taurus* species (Lin *et al.*, 2010). It is possible that the conformations observed in the holo BtADA structure are endowed by these residue substitutions. Secondly, holo HsADA2 adopts an open conformation. However, it should be noted that

the sequence similarity to HsADA2 (23% identity for BtADA and 22% for HsADA1) is low, the analogous gating helix in HsADA2 is longer and no change to a closed conformation is observed upon CF binding (Fig. 6). Finally, the catalytic pH profiles differ among HsADA1, BtADA and HsADA2; kinetic parameters as a function of pH have not been reported for MmADA. Hydrolysis of adenosine involves acid–base catalysis mediated by the Zn^{2+} cofactor, a coordinated water molecule and active-site residues Glu214 and His235. The activity of HsADA1 as a function of pH (Fig. 1) resembles the general trend of highest activity at pH \sim 6–8 as reported for BtADA (Zittle, 1946), but HsADA1 is more active than BtADA1 at higher pH values: BtADA retains 20% of its activity at pH 8.4, whereas HsADA1 retains \sim 50% of its activity at pH 9.2. In this vein, HsADA2 exhibits a pH maximum at pH \sim 6.8, and the range in which HsADA2 is active is narrower than that for HsADA1 (Zavialov & Engström, 2005). It is possible that the more sequestered active site of HsADA1 mutes the effect of solvent by limiting the pK_a perturbation of ionizable catalytic residues such as His235 and Glu214 as a function of pH, although we note that the use of different assay methods across these studies could account for some discrepancies. Finally, the slightly higher K_m of BtADA ($K_m = 43 \mu M$) for substrate compared with that of HsADA1 (measured at between 13 and 26 μM ; Wang *et al.*, 2012; Fig. 1) or MmADA (21 μM ; Sideraki *et al.*, 1996) suggests the existence of an energetic barrier associated with the conformational change needed for substrate binding.

Even though HsADA1 and MmADA do not appear to readily adopt the open conformation captured crystallographically for BtADA, there is still a need for a conformational change to allow substrate to enter the active site. Two options are likely: (i) dynamics and (ii) allosteric regulation. Supporting a role for dynamics, open and closed conformations have been extensively reported upon for a canonical TIM-barrel enzyme (Katebi & Jernigan, 2014). Upon binding, the substrate is trapped within a hydrophobic cage to facilitate catalysis. Following conversion, the product is released by the movement of peptide loops to an open conformation. Therefore, we suggest that the open conformation is a low-population excited state stabilized by the crystal lattice that is not accessed crystallographically in HsADA1. Alternatively, BtADA has been shown to be allosterically modulated in a study by Wang and coworkers that detailed the mixed inhibition mechanism of 1,3-dinitrobenzene, although it is unknown whether allosteric modulation could impose a change in the conformational of the structural gate of BtADA (Wang *et al.*, 2012; Guo & Zhou, 2016; Wodak *et al.*, 2019). Notably, the C-terminal residues common to BtADA and HsADA1 have only been observed crystallographically in the 2DA/ Ni^{2+} -bound HsADA1 structure. It is possible that there are long-range motions that propagate from these distant regions of the protein that are relevant to allostery.

The conformational state of HsADA1 is crucial in its role as an immunomodulator, as its binding to ARs has been shown to amplify both agonistic and antagonistic signaling outputs (Gracia *et al.*, 2011; Herrera *et al.*, 2001; Saura *et al.*, 1996;

Cortés *et al.*, 2015). The residues comprising the structural gate of HsADA1 and predicted AR-binding residues overlap, and previous studies have inferred or presumed that only the open conformation of HsADA1 can interact with ARs, which our structure calls into question (Gracia *et al.*, 2013; Tardif *et al.*, 2019). Firstly, holo HsADA1 has been shown to bind and amplify signaling through A_1AR and $A_{2A}AR$ (Gracia *et al.*, 2013), which we now know occurs in a closed conformation. In addition, the now-unlikely notion that MmADA converts from an open to a closed conformation upon DCF binding was used to rationalize why DCF incubation abrogates the ability of HsADA1 to amplify signaling through A_1AR and $A_{2A}AR$. Namely, HsADA1 was assumed to undergo the same open-to-closed conformational change upon DCF binding, such that its AR binding site would be distorted (Gracia *et al.*, 2013). Since a shift of the structural gate is highly unlikely, other constraints must be responsible for the lack of binding of DCF-complexed HsADA1 to A_1AR and $A_{2A}AR$. Further, HsADA1 has been shown to be able fine-tune germinal center and circulating follicular T-cell helper programs (cTfh₂₋₁₇) to improve downstream antibody production, in part due to its abilities to (i) degrade adenosine and (ii) amplify signaling through A_1AR or A_3AR (Tardif *et al.*, 2019). DCF had no effect on the impact of HsADA1 on cTfh₂₋₁₇ cells, suggesting that the binding of specific receptors may not be impacted, perhaps because no conformational change occurs. Conversely, EHNA, which is thought to stabilize an open conformation based on BtADA1 structures (Gracia *et al.*, 2013; Kinoshita *et al.*, 2008), abrogated the effect of HsADA1 on cTfh₂₋₁₇ cells (Tardif *et al.*, 2019). Overall, our structure should prompt new experiments to explore the molecular explanation for the effect of ligand complexation on the binding of HsADA1 to ARs.

In sum, the structures of holo HsADA1, BtADA and MmADA converge on the requirement for a conformational change to allow substrate binding and catalysis, but differences across the orthologs have emerged. The finding that holo HsADA1 adopts a closed conformation helps to reinterpret the conformation of holo MmADA and indicates that there is a barrier to opening the substrate gate for both enzymes. There is a possibility that the conclusions drawn from conformational changes in BtADA, which was captured in an open conformation in the absence of inhibitor in the active site, may eventually serve as a cautionary tale for the use of homologs to address functional questions on difficult biomedically relevant targets such as HsADA1 (Rodrigues *et al.*, 2013; Bolanos-Garcia & Chayen, 2009). Future studies can now focus on alternative mechanisms by which conformational changes may be triggered in HsADA1 and the relevance of these changes for interactions with binding partners such as ARs.

5. Related literature

The following reference is cited in the supporting information for this article: Pei & Grishin (2014).

Acknowledgements

We acknowledge the use of Georgia Institute of Technology Petit Institute Core Facilities.

Funding information

This work was funded by a Georgia Institute of Technology Petit Institute of Bioengineering and Biosciences seed grant to JJB and RLL. MTM is supported by NIH T32007092 and MRJ is supported by an NSF-GRFP.

References

- Bhaumik, D., Medin, J., Gathy, K. & Coleman, M. S. (1993). *J. Biol. Chem.* **268**, 5464–5470.
- Bolanos-Garcia, V. M. & Chayen, N. E. (2009). *Prog. Biophys. Mol. Biol.* **101**, 3–12.
- Bradford, K. L., Moretti, F. A., Carbonaro-Sarracino, D. A., Gaspar, M. B. & Kohn, D. B. (2017). *J. Clin. Immunol.* **37**, 626–637.
- Casañal, A., Lohkamp, B. & Emsley, P. (2020). *Protein Sci.* **29**, 1069–1078.
- Chan, B., Wara, D., Bastian, J., Hershfield, M. S., Bohnsack, J., Azen, C. G., Parkman, R., Weinberg, K. & Kohn, D. B. (2005). *Clin. Immunol.* **117**, 133–143.
- Chechik, B. E., Schrader, W. P. & Minowada, J. (1981). *J. Immunol.* **126**, 1003–1007.
- Cortés, A., Gracia, E., Moreno, E., Mallol, J., Lluís, C., Canela, E. I. & Casadó, V. (2015). *Med. Res. Rev.* **35**, 85–125.
- Fox, I. H. & Kelley, W. N. (1978). *Annu. Rev. Biochem.* **47**, 655–686.
- Gracia, E., Cortés, A., Meana, J. J., García-Sevilla, J., Hershfield, M. S., Canela, E. I., Mallol, J., Lluís, C., Franco, R. & Casadó, V. (2008). *J. Neurochem.* **107**, 161–170.
- Gracia, E., Farré, D., Cortés, A., Ferrer-Costa, C., Orozco, M., Mallol, J., Lluís, C., Canela, E. I., McCormick, P. J., Franco, R., Fanelli, F. & Casadó, V. (2013). *FASEB J.* **27**, 1048–1061.
- Gracia, E., Pérez-Capote, K., Moreno, E., Barkešová, J., Mallol, J., Lluís, C., Franco, R., Cortés, A., Casadó, V. & Canela, E. I. (2011). *Biochem. J.* **435**, 701–709.
- Guo, J. & Zhou, H.-X. (2016). *Chem. Rev.* **116**, 6503–6515.
- Herrera, C., Casadó, V., Ciruela, F., Schofield, P., Mallol, J., Lluís, C. & Franco, R. (2001). *Mol. Pharmacol.* **59**, 127–134.
- Jumper, J., Evans, R., Pritzel, A., Green, T., Figurnov, M., Ronneberger, O., Tunyasuvunakool, K., Bates, R., Židek, A., Potapenko, A., Bridgland, A., Meyer, C., Kohli, S. A. A., Ballard, A. J., Cowie, A., Romera-Paredes, B., Nikolov, S., Jain, R., Adler, J., Back, T., Petersen, S., Reiman, D., Clancy, E., Zielinski, M., Steinegger, M., Pacholska, M., Berghammer, T., Bodenstein, S., Silver, D., Vinyals, O., Senior, A. W., Kavukcuoglu, K., Kohli, P. & Hassabis, D. (2021). *Nature*, **596**, 583–589.
- Katebi, A. R. & Jernigan, R. L. (2014). *Protein Sci.* **23**, 213–228.
- Kinoshita, T., Nishio, N., Nakanishi, I., Sato, A. & Fujii, T. (2003). *Acta Cryst. D* **59**, 299–303.
- Kinoshita, T., Nakanishi, I., Terasaka, T., Kuno, M., Seki, N., Warizaya, M., Matsumura, H., Inoue, T., Takano, K., Adachi, H., Mori, Y. & Fujii, T. (2005). *Biochemistry*, **44**, 10562–10569.
- Kinoshita, T., Tada, T. & Nakanishi, I. (2008). *Biochem. Biophys. Res. Commun.* **373**, 53–57.
- Krissinel, E. & Henrick, K. (2007). *J. Mol. Biol.* **372**, 774–797.
- Kutryb-Zajac, B., Mierzejewska, P., Slominska, E. M. & Smolenski, R. T. (2020). *Molecules*, **25**, 4652.
- Lee, P. Y., Schuler, G. S., Canna, S. W., Huang, Y., Sundel, J., Li, Y., Hoyt, K. J., Blaustein, R. B., Wactor, A., Do, T., Halyabar, O., Chang, M. H., Dedeoglu, F., Case, S. M., Meidan, E., Lo, M. S., Sundel, R. P., Richardson, E. T., Newburger, J. W., Hershfield, M. S., Son, M. B., Henderson, L. A. & Nigrovic, P. A. (2020). *Ann. Rheum. Dis.* **79**, 225–231.
- Liebschner, D., Afonine, P. V., Baker, M. L., Bunkóczi, G., Chen, V. B., Croll, T. I., Hintze, B., Hung, L.-W., Jain, S., McCoy, A. J., Moriarty, N. W., Oeffner, R. D., Poon, B. K., Prisant, M. G., Read, R. J., Richardson, J. S., Richardson, D. C., Sammito, M. D., Sobolev, O. V., Stockwell, D. H., Terwilliger, T. C., Urzhumtsev, A. G., Videau, L. L., Williams, C. J. & Adams, P. D. (2019). *Acta Cryst. D* **75**, 861–877.
- Lin, B. Z., Sasazaki, S. & Mannen, H. (2010). *Anim. Sci. J.* **81**, 281–289.
- Liu, C., Skaldin, M., Wu, C., Lu, Y. & Zavialov, A. V. (2016). *Sci. Rep.* **6**, 31370.
- McCall, K. A., Huang, C. & Fierke, C. A. (2000). *J. Nutr.* **130**, 1437S–1446S.
- McCoy, A. J., Grosse-Kunstleve, R. W., Adams, P. D., Winn, M. D., Storoni, L. C. & Read, R. J. (2007). *J. Appl. Cryst.* **40**, 658–674.
- Mirdita, M., Schütze, K., Morikawa, Y., Ovchinnikov, S. & Steinegger, M. (2021). *bioRxiv*, 2021.08.15.456425.
- Mohamedali, K. A., Kurz, L. C. & Rudolph, F. B. (1996). *Biochemistry*, **35**, 1672–1680.
- Moreno, E., Canet, J., Gracia, E., Lluís, C., Mallol, J., Canela, E. I., Cortés, A. & Casadó, V. (2018). *Front. Pharmacol.* **9**, 106.
- Niu, W., Shu, Q., Chen, Z., Mathews, S., Di Cera, E. & Frieden, C. (2010). *J. Phys. Chem. B*, **114**, 16156–16165.
- Otwinowski, Z. & Minor, W. (1997). *Methods Enzymol.* **276**, 307–326.
- Pacheco, R., Martínez-Navio, J. M., Lejeune, M., Climent, N., Oliva, H., Gatell, J. M., Gallart, T., Mallol, J., Lluís, C. & Franco, R. (2005). *Proc. Natl Acad. Sci. USA*, **102**, 9583–9588.
- Pei, J. & Grishin, N. V. (2014). *Methods Mol. Biol.* **1079**, 263–271.
- Richard, E., Arredondo-Vega, F. X., Santisteban, I., Kelly, S. J., Patel, D. D. & Hershfield, M. S. (2000). *J. Exp. Med.* **192**, 1223–1236.
- Rodrigues, J. P. G. L. M., Melquiond, A. S. J., Karaca, E., Trellet, M., van Dijk, M., van Zundert, G. C. P., Schmitz, C., de Vries, S. J., Bordogna, A., Bonati, L., Kastiris, P. L. & Bonvin, A. M. J. J. (2013). *Proteins*, **81**, 2119–2128.
- Santisteban, I., Arredondo-Vega, F. X., Kelly, S., Debre, M., Fischer, A., Pérignon, J. L., Hilman, B., Eldahr, J., Dreyfus, D. H., Gelfand, E. W., Howell, P. L. & Hershfield, M. S. (1995). *Hum. Mutat.* **5**, 243–250.
- Saura, C., Ciruela, F., Casadó, V., Canela, E. I., Mallol, J., Lluís, C. & Franco, R. (1996). *J. Neurochem.* **66**, 1675–1682.
- Sideraki, V., Wilson, D. K., Kurz, L. C., Quijcho, F. A. & Rudolph, F. B. (1996). *Biochemistry*, **35**, 15019–15028.
- Tardif, V., Muir, R., Cubas, R., Chakhtoura, M., Wilkinson, P., Metcalf, T., Herro, R. & Haddad, E. K. (2019). *Nat. Commun.* **10**, 823.
- Terasaka, T., Kinoshita, T., Kuno, M., Seki, N., Tanaka, K. & Nakanishi, I. (2004). *J. Med. Chem.* **47**, 3730–3743.
- Tropea, J. E., Cherry, S. & Waugh, D. S. (2009). *Methods Mol. Biol.* **498**, 297–307.
- Tunyasuvunakool, K., Adler, J., Wu, Z., Green, T., Zielinski, M., Židek, A., Bridgland, A., Cowie, A., Meyer, C., Laydon, A., Velankar, S., Kleywegt, G. J., Bateman, A., Evans, R., Pritzel, A., Figurnov, M., Ronneberger, O., Bates, R., Kohli, S. A. A., Potapenko, A., Ballard, A. J., Romera-Paredes, B., Nikolov, S., Jain, R., Clancy, E., Reiman, D., Petersen, S., Senior, A. W., Kavukcuoglu, K., Birney, E., Kohli, P., Jumper, J. & Hassabis, D. (2021). *Nature*, **596**, 590–596.
- Uhlén, M., Fagerberg, L., Hallström, B. M., Lindskog, C., Oksvold, P., Mardinoglu, A., Sivertsson, A., Kampf, C., Sjödéd, E., Asplund, A., Olsson, I., Edlund, K., Lundberg, E., Navani, S., Szgyarto, C. A., Odeberg, J., Djureinovic, D., Takanen, J. O., Hober, S., Alm, T., Edqvist, P. H., Berling, H., Tegel, H., Mulder, J., Rockberg, J., Nilsson, P., Schwenk, J. M., Hamsten, M., von Feilitzen, K., Forsberg, M., Persson, L., Johansson, F., Zwahlen, M., von Heijne, G., Nielsen, J. & Pontén, F. (2015). *Science*, **347**, 1260419.
- Van der Weyden, M. B. & Kelley, W. N. (1976). *J. Biol. Chem.* **251**, 5448–5456.

- Wang, Y., Liu, X., Schneider, B., Zverina, E. A., Russ, K., Wijeyesakere, S. J., Fierke, C. A., Richardson, R. J. & Philbert, M. A. (2012). *Toxicol. Sci.* **125**, 509–521.
- Wang, Z. & Quioco, F. A. (1998). *Biochemistry*, **37**, 8314–8324.
- Wiginton, D. A., Kaplan, D. J., States, J. C., Akeson, A. L., Perme, C. M., Bilyk, I. J., Vaughn, A. J., Lattier, D. L. & Hutton, J. J. (1986). *Biochemistry*, **25**, 8234–8244.
- Wilkins, M. R., Gasteiger, E., Bairoch, A., Sanchez, J. C., Williams, K. L., Appel, R. D. & Hochstrasser, D. F. (1999). *Methods Mol. Biol.* **112**, 531–552.
- Wilson, D. K. & Quioco, F. A. (1993). *Biochemistry*, **32**, 1689–1694.
- Wodak, S. J., Paci, E., Dokholyan, N. V., Berezovsky, I. N., Horovitz, A., Li, J., Hilser, V. J., Bahar, I., Karanicolas, J., Stock, G., Hamm, P., Stote, R. H., Eberhardt, J., Chebaro, Y., Dejaegere, A., Cecchini, M., Changeux, J. P., Bolhuis, P. G., Vreede, J., Faccioli, P., Orioli, S., Ravasio, R., Yan, L., Brito, C., Wyart, M., Gkeka, P., Rivalta, I., Palermo, G., McCammon, J. A., Panecka-Hofman, J., Wade, R. C., Di Pizio, A., Niv, M. Y., Nussinov, R., Tsai, C. J., Jang, H., Padhorny, D., Kozakov, D. & McLeish, T. (2019). *Structure*, **27**, 566–578.
- Zavialov, A. V. & Engström, A. (2005). *Biochem. J.* **391**, 51–57.
- Zavialov, A. V., Gracia, E., Glaichenhaus, N., Franco, R., Zavialov, A. V. & Lauvau, G. (2010). *J. Leukoc. Biol.* **88**, 279–290.
- Zavialov, A. V., Yu, X., Spillmann, D., Lauvau, G. & Zavialov, A. V. (2010). *J. Biol. Chem.* **285**, 12367–12377.
- Zittle, C. A. (1946). *J. Biol. Chem.* **166**, 499–503.